

A Model for Numerical Simulation of Heat and Water Vapor Exchange in Multilayer Textile Packages With three-dimensional Spacer Fabrics Ventilation Layer

Rimantas Barauskas and Ausra Abraitiene

Textile Research Journal published online 15 June 2011

DOI: 10.1177/0040517510392468

The online version of this article can be found at:
<http://trj.sagepub.com/content/early/2011/06/01/0040517510392468>

Published by:



<http://www.sagepublications.com>

Additional services and information for *Textile Research Journal* can be found at:

Email Alerts: <http://trj.sagepub.com/cgi/alerts>

Subscriptions: <http://trj.sagepub.com/subscriptions>

Reprints: <http://www.sagepub.com/journalsReprints.nav>

Permissions: <http://www.sagepub.com/journalsPermissions.nav>

A model for numerical simulation of heat and water vapor exchange in multilayer textile packages with three-dimensional spacer fabric ventilation layer

Rimantas Barauskas¹ and Ausra Abraitiene²

Textile Research Journal

0(00) 1–21

© The Author(s) 2010

Reprints and permissions:

sagepub.co.uk/journalsPermissions.nav

DOI: 10.1177/0040517510392468

trj.sagepub.com



Abstract

The work presents a structural computational model developed for investigation of heat and air–water vapor mass exchange between the multilayer textile packages and the human body. Each fabric layer is represented by a single element, characterized by its air and water vapor permeability, thermal resistance and heat capacity, as well as, water vapor absorption properties. While characteristics of each layer are obtained experimentally, the computational model enables the prediction of the variation in time of temperature and humidity in the gaps between each pair of adjacent layers. The finite element, which represents the forced ventilation layer made of three-dimensional textile material, is created and may be used as a structural element within the overall structural model of the textile package. The element equations are derived on the basis of ideal gas state equation. The results of the measured textile layers characteristics and the numerical data are presented. Though the condensation of water vapor was not considered in this model, the time point of initiation of sweating at given heat and water vapor generation rates could be predicted.

Keywords

Textile multi-layers, ventilation, thermal and moisture transport, finite element modeling

Multi-layer textile packages (MTP) are widely used for protection against ballistic impacts and influences of dangerous environments.¹ MTP of a new generation enable lower surface density and better functionality to be achieved by using new textile materials, which employ integrated smart sensors and/or refrigeration structures. New technologies based on lamination and thermoplastic film creation enable many desirable effects providing necessary ballistic protection to be achieved, along with the considerable improvement in wearing comfort. One of the important challenges for ballistic protection clothing designers is to ensure the wearing comfort by providing necessary thermal and moisture concentration balance at the human skin surface (microclimate layer).

Theoretical investigations of the physical behavior of new generation textiles are complicated because of the very complex internal structure, coupled with heat and moisture transfer and other physical processes, which occur in different space and time scales. During the last decade numerous researches have been carried out

regarding the mathematical modeling of different aspects of physical behavior of fabric structures. The models described by Li and Zhu² analyzed the simultaneous heat and moisture transfer in porous textiles with phase change materials (PCM). The model of micro-PCM has been introduced and the slab of textiles treated as a continuum model by using the finite volume method. By using the finite volume difference scheme, the thermal buffering effect of PCM is simulated. The distributions of temperature and moisture concentration in porous textiles with PCM are numerically computed by this technique. The research has been carried

¹Kaunas University of Technology, Lithuania.

²Lithuanian Textiles Institute, Lithuania.

Corresponding author:

Rimantas Barauskas, Kaunas University of Technology, Studentu Str. 50-407, Kaunas 51368, Lithuania
Email: rimantas.barauskas@ktu.lt

out at the micro-level by considering heat and moisture exchange processes in a yarn.

In the model³ the moisture absorption of fibers and the effects of the phase transition temperature range, as well as the heating/cooling rate on the phase change processes of the PCM, were considered. The theoretical predictions were validated by experimental data.

Ren and Ruckman⁴ investigated the behavior of condensation in three-layer waterproof breathable fabrics for clothing. The water vapor transfer when condensation occurs within the three-layer waterproof breathable fabrics has been based on the simultaneous heat and mass transfer theory. It was demonstrated that the condensation problem may be solved by changing some physical properties of a three-layer waterproof breathable fabric.

Models considering natural ventilation in clothes have been formulated by Ghaddar et al.⁵⁻⁷ Clothing contact with a human body has been presented by means of two non-concentric cylinder systems, where the internal one can move thus imitating the microclimate gap change in wearing conditions of walking humans. The equations describe the motion of the air and water vapor within the gap simultaneously with the heat transfer by means of conduction and convection. A description was also given of the means by which the fabric and fabric-to-skin macroscopic heat and mass transfer internal transport coefficients could be determined.

The experiments described by Oh⁸ were designed to test the water vapor transfer rates through a clothing system with an air gap between layers, under conditions closer to actual wear. The water vapor transfer and condensation effects in textile multi-layers have been experimentally analyzed.⁹ Hydrophilic and hydrophobic layer combinations were used in order to achieve the desirable moisture absorption effect of the multilayer.

The equations of thermal conduction and moisture diffusion in a unit cell of a fibrous material, as well as, in a unit cell of a woven fabric have been formulated.¹⁰ By applying the homogenization method, the equations were extended to be applied to finite size domains of the fabric. The work was theoretical and aimed to develop a mathematical background for further development of numerical solution schemes.

A mathematical model, which considers the woven fabric as a system of porous yarns, interlacements between warp and weft yarns and air pores and all the basic weaves in order to predict the thermal resistance of fabrics has been presented by Bhattacharjee and Kothari.¹¹ The conduction and radiation heat transfer together, was calculated based on the construction parameters of the fabric. The thermal insulation, which is equivalent to the thermal resistance, was predicted with the help of these parameters.

Experimental measurement procedures and equipment of water vapor resistance of textile layers is determined by appropriate standards, however, such measurements often do not provide all necessary data and relationships, which are necessary for the development of advanced mathematical models. Many recent publications are devoted to the enhancement of experimental techniques and procedures. Fukazawa et al.¹² referred to new apparatus, which was developed for measuring water vapor permeability.

Modern textile technology provides many unique solutions for requirements on fibrous material configuration and construction and therefore properties, and its capability for creating various volumetric (three-dimensional) textile architectures has caused tremendous interest for advanced technical applications in, for example, the aerospace and automotive industries. Three-dimensional textiles¹³ are made of two layers of knitted material, which are connected together by mono-filament links comprising a three-dimensional structure. Its thickness may vary from 1.5 mm to 60 mm. While thinner structures are suitable for clothes, the thick structures are used in vehicle and building industry. Three-dimensional textiles are breathable, with temperature regulating properties, are compression resistant, have good physiological properties and are soft, have moisture-transporting ability and good surface resistance. In this investigation we used the three-dimensional textile as a forced ventilation layer positioned between the multilayer textile package and human body.

This work presents a new structural model for computational modeling of the heat and water vapor exchange process through textile multi-layers and is an extension of the model that originated from our earlier paper.¹⁴ The equations are formulated for an element, which represents a single textile layer with nodes situated in the inter-layer air gaps. The equations of elements are assembled to the structural equation in accordance with the standard discrete system approach.¹⁵ Air and water vapor mass and heat transport, as well as, convective heat exchange through the layers of the textile package has been described by using appropriate water vapor transmission and heat conduction coefficients as physical constants. In addition, a model of the forced ventilation layer made of three-dimensional textiles has been described. The equations were presented in a form that enabled the assembly of the ventilation layer element together with other textile layers elements and to form the overall structural equation system of the hybrid textile package. The water vapor condensation process is not included in the model, therefore only the point of the initiation of condensation could be investigated. Results of numerical and physical experiments are presented.

Flow rate and heat balance equations of textile layer

The scheme of water vapor and air flow within the textile layer finite element is presented in Figure 1a. Two nodes of the element are situated in air gaps between the adjacent textile layers. The nodal variables of the element are masses, m_{v1} , m_{v2} , of water vapor and masses, m_{a1} , m_{a2} , of the air in the gaps, as well as, temperatures, T_1 , T_2 , in the gaps. The geometry of

the element is described by textile layer thickness, h_t , sizes of the gaps, h_{g1} , h_{g2} , and area of the textile layer, A . The water vapor and air partial pressures, p_{v1} , p_{a1} , p_{v2} , p_{a2} , in the gaps can be expressed in terms of nodal variables and geometrical parameters of the element as

$$\begin{aligned}
 p_{a1} &= \frac{m_{a1}RT_1}{\mu_a h_{g1}A}, & p_{v1} &= \frac{m_{v1}RT_1}{\mu_v h_{g1}A}, \\
 p_{a2} &= \frac{m_{a2}RT_2}{\mu_a h_{g2}A}, & p_{v2} &= \frac{m_{v2}RT_2}{\mu_v h_{g2}A},
 \end{aligned}
 \tag{1}$$

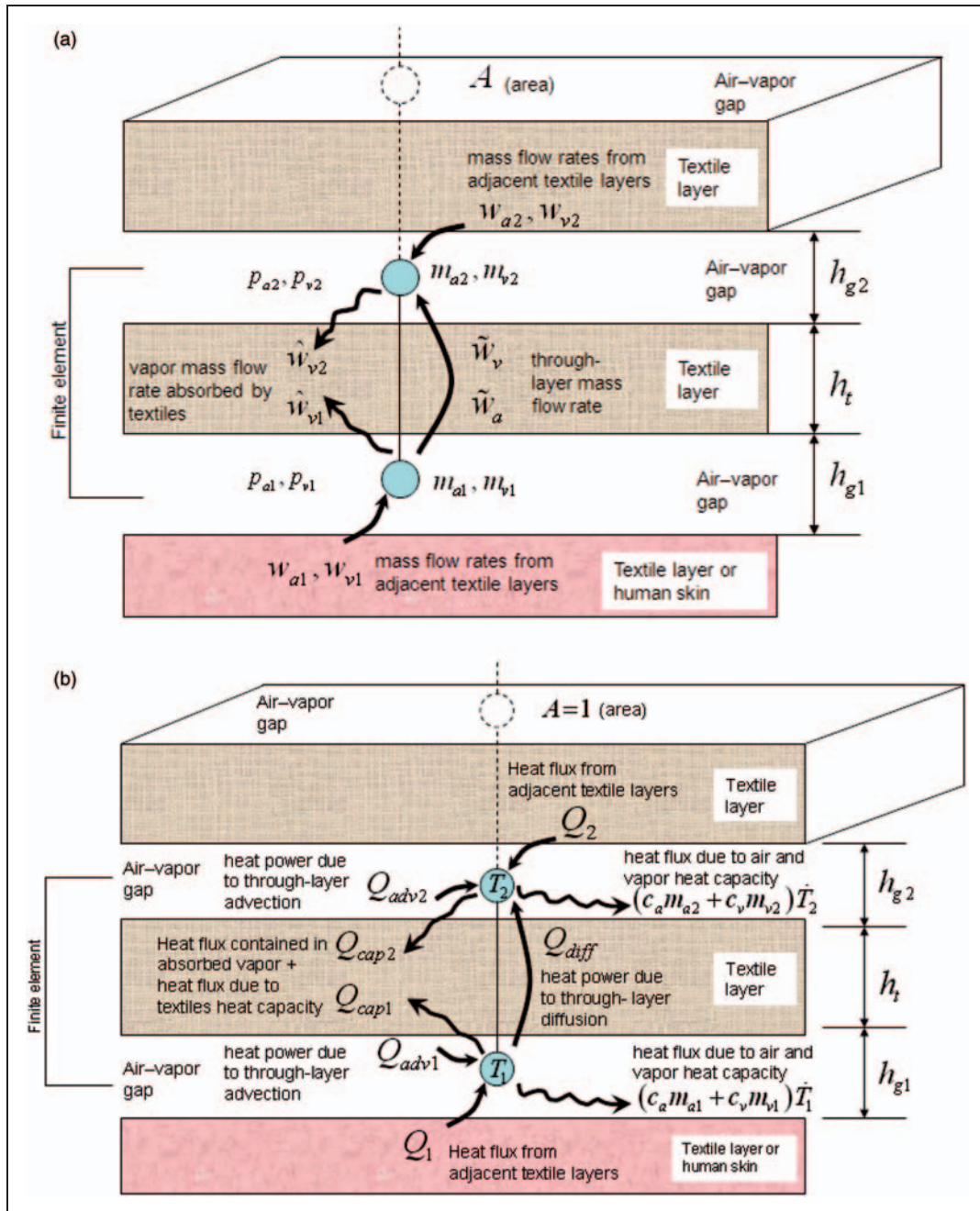


Figure 1. Flow rates of air and water vapor (a) and heat fluxes (b) in the textile layer element.

where $\mu_v = 0.018 \text{ kg}$, $\mu_a = 0.029 \text{ kg}$, molar masses of water vapor and air; $R = 8.314472 \text{ Jmol}^{-1}\text{K}^{-1}$, the universal gas constant.

We assume that the overall heat and mass exchange mechanism in the textile multilayer consists of several physical processes, which take part simultaneously. The pressures, p_{v1} , p_{a1} , p_{v2} , p_{a2} , in the gaps at both sides of the textile layer may have different values. Therefore the gas (water vapor and air mixture) may penetrate through the textile layer, as well as, some quantity of the water vapor may be accumulated in the textile layer. The heat is transferred by convection because of the gas motion. Simultaneously, a certain amount of heat is transferred through the textile layer by means of conduction and convection heat exchange mechanisms. In our model we describe the mass and heat exchange processes by means of flow rate balance equations and heat balance equations.

The air and water vapor flow rates at both nodes of the finite element considered in the balance equations are as follows:

1. \hat{w}_{v1} , \hat{w}_{v2} , the flow rates of water vapor, which is accumulated in the yarns of the textile layer. We assume that the flow rates are directly proportional to the rates of change of the water vapor partial pressure as

$$\hat{w}_{v1} = \frac{1}{2} A c_{ht} \dot{p}_{v1}; \quad \hat{w}_{v2} = \frac{1}{2} A c_{ht} \dot{p}_{v2}, \quad (2)$$

where c_{ht} is the hydraulic capacity of the textile layer, which describes the ability of the unit area of the textile layer to accumulate the water vapor. The coefficients '1/2' on the right-hand sides of both Equations (2) mean that the water vapor accumulation is equally influenced by pressure changes in both gaps;

2. \tilde{w}_v , \tilde{w}_a are the flow rates of water vapor and air penetrating through the textile layer because of different pressure values in the gaps at the bottom and the top of the layer. The flow rates are assumed to be proportional to the differences of partial pressures of water vapor and air in the gaps at both sides of the textile layer and are expressed as

$$\tilde{w}_v = \delta_p A (p_{v1} - p_{v2}); \quad \tilde{w}_a = k_a A (p_{a1} - p_{a2}), \quad (3)$$

where δ_p is the water vapor transmission coefficient, k_a is the air permeability coefficient;

3. w_{a1} , w_{v1} , w_{a2} , w_{v2} are the flow rates of water vapor and air transferred to the gaps from the adjacent textile layers. After the element equations are assembled into structural equations, such inter-element flow rates add up to zero or to the values of the

externally supplied flow rates because of the balance condition at each node of the structure.

The scheme of the heat exchange within the textile layer finite element is presented in Figure 1b. The heat fluxes considered in the thermal balance equations are as follows:

1. Q_{diff} , the diffusive heat flux through the textile layer determined by the combined conduction-convection heat transfer mechanism expressed as

$$Q_{diff} = \alpha_t A (T_1 - T_2), \quad (4)$$

where α_t is the heat transfer coefficient of the unity area of the textile layer. The coefficient α_t , represents the combined heat transfer capability of the layer, which includes the convective heat exchange between the gas in the gaps and the yarns (or laminate) of textiles, as well as, the diffusive (i.e. conduction-type) heat flux through the textile material. In fact such a coefficient is obtained directly (or is recalculated) by using the standard measurement procedures;

2. Q_{cap1} , Q_{cap2} , the heat fluxes created by the flow rates of water vapor, which is accumulated in the yarns of the textile layer, and by the thermal capacity of the textile layer as

$$Q_{cap1} = c_v \hat{w}_{v1} T_1 + \frac{A}{2} c_t \dot{T}_1; \quad Q_{cap2} = c_v \hat{w}_{v2} T_2 + \frac{A}{2} c_t \dot{T}_2, \quad (5)$$

where c_v is the specific (mass) heat capacity coefficient of water vapor, c_t is the heat capacity of the unity area of the textile layer.

3. Q_{adv1} , Q_{adv2} , the convection heat fluxes at both sides of the textile layer created by the water vapor and air flow rates from the textile layer to the inter-layer gaps. The values of the fluxes depend on the direction of the air and water vapor flow through the textile layer (assumed positive directions of the flow rates are indicated in Figure 1a). The expressions of the fluxes read as:

$$Q_{adv1} = \begin{cases} \text{if } \tilde{w}_v < 0, & c_v |\tilde{w}_v| T_2, & \text{else,} & -c_v |\tilde{w}_v| T_1; \\ \text{if } \tilde{w}_a < 0, & c_a |\tilde{w}_a| T_2, & \text{else,} & -c_a |\tilde{w}_a| T_1; \end{cases}$$

$$Q_{adv2} = \begin{cases} \text{if } \tilde{w}_v > 0, & c_v |\tilde{w}_v| T_1, & \text{else,} & -c_v |\tilde{w}_v| T_2; \\ \text{if } \tilde{w}_a > 0, & c_a |\tilde{w}_a| T_1, & \text{else,} & -c_a |\tilde{w}_a| T_2, \end{cases} \quad (6)$$

where $(c_a m_{a1} + c_v m_{v1}) \dot{T}_1$, $(c_a m_{a2} + c_v m_{v2}) \dot{T}_2$ are the heat fluxes due to heat capacity of air and water vapor contained in the gaps between the layers.

4. Q_1, Q_2 , the heat fluxes from the adjacent textile layers. After the element equations are assembled into the structural equations, such ‘inter-element’ fluxes add up to zero or to the value of the externally supplied heat flux because of the thermal balance conditions at each node of the structure.

The positive directions of the flow rates and heat fluxes are presented in Figures 1a and b. The finite element equations are derived by using the principle of balance of incoming and outgoing flow rates and heat fluxes at each node. At the bottom node of the element the rate of change of the mass of the water vapor equals the algebraic sum of all mass flow rates of the water vapor supplied to or withdrawn from the bottom gap as $\dot{m}_{v1} = w_{v1} - \tilde{w}_v - \hat{w}_{v1}$. An analogous equation is valid for the rate of change of the mass of the air as $\dot{m}_{a1} = w_{a1} - \tilde{w}_a$. All the aforementioned heat fluxes, $Q_1, Q_{cap1}, Q_{diff}, Q_{adv1}$ and $(c_a m_{a1} + c_v m_{v1})\dot{T}_1$, which are transferred to or withdrawn from the bottom gap add up to zero. Finally the flow rate and heat flux balance equations of the bottom node of the element read as

$$\begin{cases} w_{v1} - \tilde{w}_v - \hat{w}_{v1} - \dot{m}_{v1} = 0; \\ w_{a1} - \tilde{w}_a - \dot{m}_{a1} = 0; \\ Q_1 - (c_a m_{a1} + c_v m_{v1})\dot{T}_1 - Q_{cap1} - Q_{diff} + Q_{adv1} = 0. \end{cases} \quad (7)$$

$$\left[\begin{array}{cc|cc} \frac{c_{ht}RT_1}{2\mu_v h_{g1}} + 1 & 0 & \frac{c_{ht}R}{2\mu_v h_{g1}} m_{v1} & 0 \\ 0 & 1 & 0 & 0 \\ \frac{c_v c_{ht}R}{2\mu_v h_{g1}} (T_1)^2 & 0 & c_a m_{a1} + c_v m_{v1} + \frac{c_v c_{ht}R}{2\mu_v h_{g1}} m_{v1} T_1 + \frac{Ac_t}{2} & 0 \\ 0 & 0 & 0 & 0 \\ 0 & 0 & 0 & 0 \\ 0 & 0 & 0 & 0 \end{array} \right] \begin{bmatrix} \dot{m}_{v1} \\ \dot{m}_{a1} \\ \dot{T}_{v1} \\ \dot{m}_{v2} \\ \dot{m}_{a2} \\ \dot{T}_{v2} \end{bmatrix} = \begin{bmatrix} -\delta_p A(p_{v1} - p_{v2}) \\ -k_a A(p_{a1} - p_{a2}) \\ -\alpha_t A(T_1 - T_2) + Q_{adv1} \\ \delta_p A(p_{v1} - p_{v2}) \\ k_a A(p_{a1} - p_{a2}) \\ \alpha_t A(T_1 - T_2) + Q_{adv2} \end{bmatrix} + \begin{bmatrix} w_{v1} \\ w_{a1} \\ Q_1 \\ w_{v2} \\ w_{a2} \\ Q_2 \end{bmatrix}; \quad (10)$$

Similar consideration is valid for the top node, the balanced equations of which read as

$$\begin{cases} w_{v2} + \tilde{w}_v - \hat{w}_{v2} - \dot{m}_{v2} = 0; \\ w_{a2} + \tilde{w}_a - \dot{m}_{a2} = 0; \\ Q_2 - (c_a m_{a2} + c_v m_{v2})\dot{T}_2 - Q_{cap2} + Q_{diff} = 0. \end{cases} \quad (8)$$

Equation systems (7) and (8) provide the base for the flow rate and heat flux balance equation system of the finite element. All variables of (7) and (8) have to be expressed in terms of $m_{v1}, m_{a1}, T_1, m_{v2}, m_{a2}, T_2$, which are the nodal variables of the finite element. After substituting expressions (2)–(6) into Equations (7) and (8) the equation system of the finite element reads as

$$\begin{cases} w_{v1} - \delta_p A(p_{v1} - p_{v2}) - \frac{Ac_{ht}}{2} \dot{p}_{v1} - \dot{m}_{v1} = 0; \\ w_{a1} - k_a A(p_{a1} - p_{a2}) - \dot{m}_{a1} = 0; \\ Q_1 - (c_a m_{a1} + c_v m_{v1})\dot{T}_1 - \frac{A}{2} (c_v c_{ht} T_1 \dot{p}_{v1} + c_t \dot{T}_1) - \alpha_t A(T_1 - T_2) + Q_{adv1} = 0; \\ w_{v2} + \delta_p A(p_{v1} - p_{v2}) - \frac{Ac_{ht}}{2} \dot{p}_{v2} - \dot{m}_{v2} = 0; \\ w_{a2} + k_a A(p_{a1} - p_{a2}) - \dot{m}_{a2} = 0; \\ Q_2 - (c_a m_{a2} + c_v m_{v2})\dot{T}_2 - \frac{A}{2} (c_v c_{ht} \dot{p}_{v2} T_2 + c_t \dot{T}_2) + \alpha_t A(T_1 - T_2) + Q_{adv2} = 0; \end{cases} \quad (9)$$

Finally, substitution of relationship (1) into (9) and appropriate algebraic manipulations enable the expression of pressures in terms of temperatures and masses and lead to the element equation in the matrix form as

where Q_{adv1}, Q_{adv2} are calculated by using expressions (6).

The rightmost vector of Equation (10) presents the nodal flow rates and heat fluxes $w_{v1}, w_{a1}, Q_1, w_{v2}, w_{a2}, Q_2$, which are transferred to the nodes of the finite element from adjacent elements. At the moment they are

unknown as flow rate and heat flux balance equations of a single finite element are considered. However, after assembling the equation system of the structure, the inter-element flow rates and heat fluxes are eliminated or replaced by the known externally applied flow rates and heat fluxes.

Diagonal terms $(c_a m_{a1} + c_v m_{v1})\dot{T}_1$, $(c_a m_{a2} + c_v m_{v2})\dot{T}_2$ of the left-hand side matrix in Equation (10) are the capacity terms corresponding to inter-layer gaps, which are common to each pair of the elements of the textile package structure. As the equations of individual elements are joined together to the equation system of the structure, the terms should be added directly to the appropriate positions in the diagonal of the assembled structural capacity matrix of the structure rather than being 'assembled' from the matrices of individual finite elements.

Flow rate and heat balance equations of the three-dimensional textile ventilation layer

The ~7.5 mm thickness ventilation layer is made of three-dimensional textile and is situated between the human body and the textile multilayer. The forced air flow created by means of a ventilator is supplied to the inlet of the ventilation layer. In our model the finite element of the ventilation layer is formulated as follows. The ventilation layer finite element has three nodes, two of which are situated in the gaps at the bottom and top of the three-dimensional textile layer and the third node which represents the inside of the ventilation layer, Figure 2. The temperatures and partial pressures of air and water vapor at the surface of the human body and between the three-dimensional layer and the rest of the multilayer textile package are assumed to be different from the temperature of the ventilation airflow. The mass and heat exchange takes place between the air and water vapor contained in gaps at the nodes of the element and at the internal node of the three-dimensional ventilation layer.

The scheme of water vapor and air flow within the ventilation finite element is presented in Figure 2a. The nodal variables of the finite element are masses, m_{v1} , m_{v2} , m_{v0} , of water vapor and masses, m_{a1} , m_{a2} , m_{a0} , of the air contained in the inter-layer gaps and within the ventilation layer, as well as, temperatures T_1 , T_2 , T_0 in the inter-layer gaps and in the ventilation layer. The geometry of the element is described by sizes h_{g1} , h_{g2} of the gaps, the ventilation layer thickness, h_0 , and area, A . The water vapor and air partial pressures p_{v1} , p_{a1} , p_{v2} , p_{a2} , p_{v0} , p_{a0} in the gaps and in the ventilation layer can be expressed in terms of nodal variables by using relations (1).

The sequence of writing equations for the ventilation element is similar to that employed in the previous section, where the textile layer element equations have

been derived. The flow rates considered in the flow rate and heat flux balance equations are:

1. \tilde{w}_{v1} , \tilde{w}_{a1} , \tilde{w}_{v2} , \tilde{w}_{a2} , the flow rates of water vapor and air through the bottom and top surfaces of the three-dimensional ventilation layer to the gaps at both sides of the ventilation layer caused by different pressure values in the gaps and within the layer. The flow rates are assumed to be proportional to the partial pressures of water vapor and air as

$$\begin{aligned}\tilde{w}_{v1} &= \tilde{\delta}_p A(p_{v1} - p_{v0}); & \tilde{w}_{a1} &= \tilde{k}_a A(p_{a1} - p_{a0}); \\ \tilde{w}_{v2} &= \tilde{\delta}_p A(p_{v2} - p_{v0}); & \tilde{w}_{a2} &= \tilde{k}_a A(p_{a2} - p_{a0}),\end{aligned}\quad (11)$$

where $\tilde{\delta}_p$, \tilde{k}_a are the water vapor transmission coefficient and air permeability coefficient of the ventilation layer, respectively.

2. w_{a1} , w_{v1} , w_{a2} , w_{v2} , the flow rates of water vapor and air obtained from adjacent textile layers or from the human skin. After the element equations are assembled to structural equations, such 'inter-element' flow rates add up to zero or to a value of an externally supplied flow rate because of the flow rate and heat flux balance condition at each node of the structure;
3. w_{a0}^+ , w_{v0}^+ , the flow rates of water vapor and air supplied to the inlet of the ventilation layer by the ventilator;
4. w_{a0}^- , w_{v0}^- , the flow rates of water vapor and air leaving the ventilation layer through the outlet.

The scheme of the heat exchange within the ventilation layer finite element is presented in Figure 2b. The heat fluxes considered in the thermal balance equations are as follows:

1. Q_{diff12} , the diffusive heat flux determined by the thermal conductivity of the solid structure of the ventilation layer as

$$Q_{diff12} = \alpha_{3D} A(T_1 - T_2), \quad (12)$$

where α_{3D} is the heat transfer coefficient, which is used to quantify the basically diffusive heat flux Q_{diff12} between the nodes 1 and 2 at both sides of the ventilation layer through the solid structure of the ventilation layer. Note that heat flux Q_{diff12} is directed from node 1 to 2 by omitting node 0. It does not represent the convective heat fluxes caused by air and water vapor flow rates;

2. Q_{conv10} , Q_{conv20} , the convective heat fluxes through the bottom and top surfaces of the ventilation layer determined as

$$\begin{aligned}Q_{conv20} &= \tilde{\alpha}_{3D} A(T_2 - T_0); \\ Q_{conv10} &= \tilde{\alpha}_{3D} A(T_1 - T_0),\end{aligned}\quad (13)$$

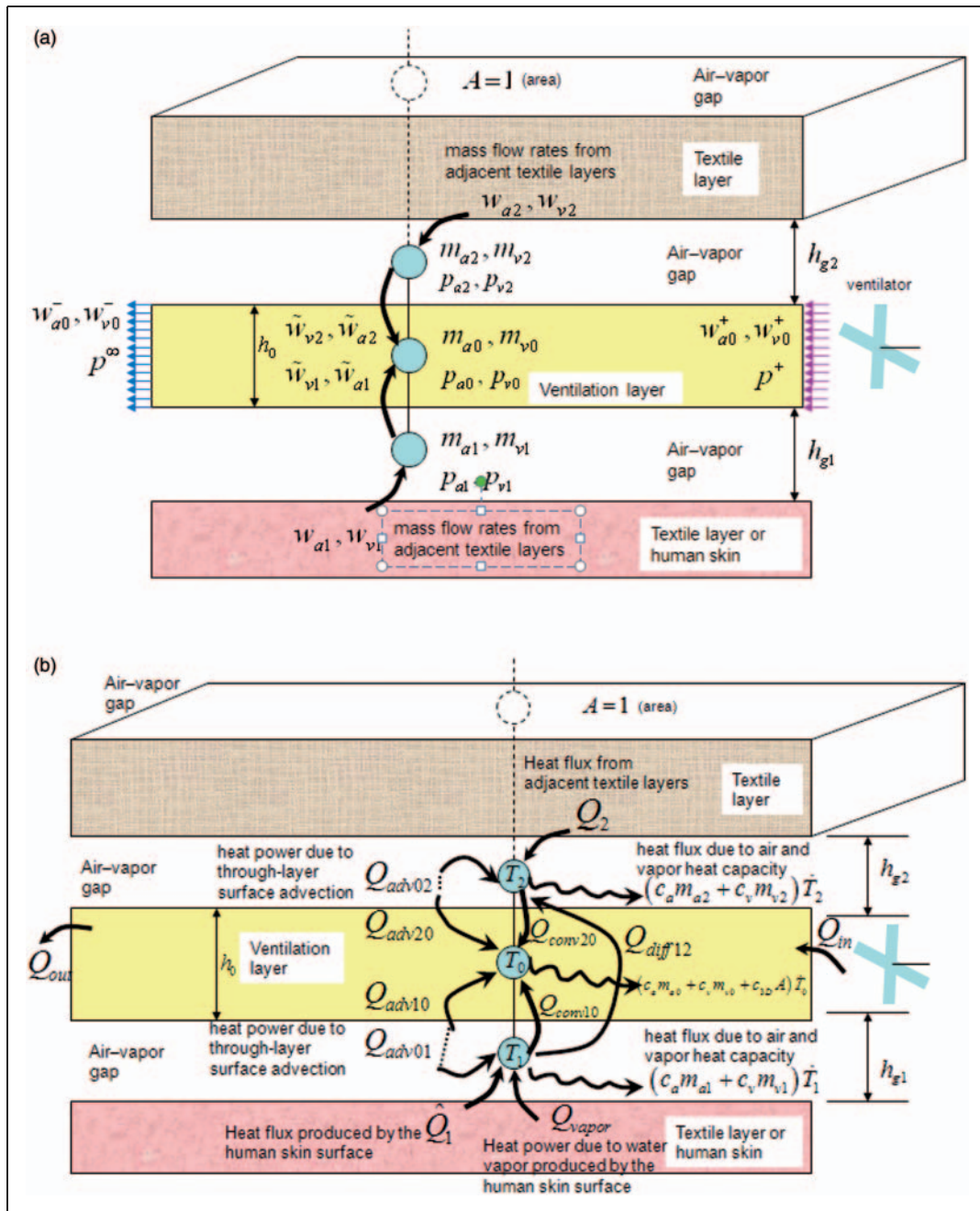


Figure 2. Flow rates of air and water vapor (a) and heat fluxes (b) in the ventilation layer element.

where $\tilde{\alpha}_{3D}$ is the convective heat transfer coefficient. The heat transfer coefficient $\tilde{\alpha}_{3D}$ is used in order to quantify the convective heat exchange between three-dimensional textile material, which is the solid structure containing water vapor and air and the neighboring air-water vapor gas mixture in the inter-layer gap;

3. Q_{adv01}, Q_{adv10} , the convection heat fluxes at both sides of the textile layer created by the water vapor and air flow rates through the bottom surface of the three-dimensional layer. The values of the fluxes

depend on the direction of air and water vapor flow through the surface (assumed positive directions of the flow rates are indicated in Figure 2a) as

$$\begin{aligned}
 Q_{adv01} &= \begin{cases} \text{if } \tilde{w}_{v1} > 0, & -c_v |\tilde{w}_{v1}| T_1, \text{ else, } c_v |\tilde{w}_{v1}| T_0; \\ \text{if } \tilde{w}_{a1} > 0, & -c_a |\tilde{w}_{a1}| T_1, \text{ else, } c_a |\tilde{w}_{a1}| T_0; \end{cases} \\
 Q_{adv10} &= \begin{cases} \text{if } \tilde{w}_{v1} > 0, & c_v |\tilde{w}_{v1}| T_1, \text{ else, } -c_v |\tilde{w}_{v1}| T_0; \\ \text{if } \tilde{w}_{a1} > 0, & c_a |\tilde{w}_{a1}| T_1, \text{ else, } -c_a |\tilde{w}_{a1}| T_0; \end{cases} \quad (14)
 \end{aligned}$$

4. Q_{adv02} , Q_{adv20} , the convection heat fluxes at both sides of the textile layer created by the water vapor and air flow rates through the top surface of the three-dimensional layer. The values of the fluxes depend on the direction of air and water vapor flow through the surface as

$$Q_{adv02} = \begin{cases} \text{if } \tilde{w}_{v2} > 0, & -c_v|\tilde{w}_{v2}|T_2, \text{ else, } c_v|\tilde{w}_{v2}|T_0; \\ \text{if } \tilde{w}_{a2} > 0, & -c_a|\tilde{w}_{a2}|T_2, \text{ else, } c_a|\tilde{w}_{a2}|T_0; \end{cases}$$

$$Q_{adv20} = \begin{cases} \text{if } \tilde{w}_{v2} > 0, & c_v|\tilde{w}_{v2}|T_2, \text{ else, } -c_v|\tilde{w}_{v2}|T_0; \\ \text{if } \tilde{w}_{a2} > 0, & c_a|\tilde{w}_{a2}|T_2, \text{ else, } -c_a|\tilde{w}_{a2}|T_0; \end{cases} \quad (15)$$

5. $(c_a m_{a1} + c_v m_{v1})\dot{T}_1$, $(c_a m_{a2} + c_v m_{v2})\dot{T}_2$, $(c_a m_{a0} + c_v m_{v0} + c_{3D}A)\dot{T}_0$, heat fluxes due to heat capacity of air and water vapor contained in gaps between textile layers and in three-dimensional layer, as well as, in the heat capacity of the structure of three-dimensional layer;

6. Q_1 , Q_2 , the heat fluxes from the adjacent textile layers. As the ventilation layer is the first element of the structure situated at the human skin, Q_1 represents the heat power \hat{Q}_1 produced by the human skin and the heat power $Q_{vapqr} = c_v \hat{w}_{v1} T_{human}$ contained in the mass flow rate, \hat{w}_{v1} , of the generated water vapor:

$$Q_1 = \hat{Q}_1 + c_v \hat{w}_{v1} T_{human}. \quad (16)$$

7. Q_{in} , Q_{out} , the heat power contained in the mass flow rates, w_{v0}^+ , w_{a0}^+ , w_{v0}^- , w_{a0}^- , through the inlet and outlet of the ventilation layer obtained as

$$Q_{in} = (c_v w_{v0}^+ + c_a w_{a0}^+) T^+; \quad (17)$$

$$Q_{out} = (c_v w_{v0}^- + c_a w_{a0}^-) T_0,$$

where T^+ is the temperature of the air and water vapor mixture at the inlet of the ventilation layer.

The directions of the flow rates and heat fluxes are presented in Figure 2a and b. Similarly as explained in the previous section, the finite element equations are derived by using the principle of balance of incoming and outgoing flow rates and heat fluxes at each node as

$$\begin{cases} \tilde{w}_{v1} + \tilde{w}_{v2} + w_{v0}^+ - w_{v0}^- - \dot{m}_{v0} = 0; \\ \tilde{w}_{a1} + \tilde{w}_{a2} + w_{a0}^+ - w_{a0}^- - \dot{m}_{a0} = 0; \\ Q_{diff10} + Q_{diff20} + Q_{adv10} + Q_{adv20} \\ - (c_a m_{a0} + c_v m_{v0})\dot{T}_0 + Q_{in} - Q_{out} = 0; \end{cases} \quad (18)$$

at the central node,

$$\begin{cases} w_{v1} - \tilde{w}_{v1} - \dot{m}_{v1} = 0; \\ w_{a1} - \tilde{w}_{a1} - \dot{m}_{a1} = 0; \\ \hat{Q}_1 + c_v \hat{w}_{v1} T_{human} - (c_a m_{a1} + c_v m_{v1})\dot{T}_1 \\ - Q_{diff10} - Q_{diff12} + Q_{adv01} = 0 \end{cases} \quad (19)$$

at the bottom node and

$$\begin{cases} w_{v2} - \tilde{w}_{v2} - \dot{m}_{v2} = 0; \\ w_{a2} - \tilde{w}_{a2} - \dot{m}_{a2} = 0; \\ Q_2 - (c_a m_{a2} + c_v m_{v2})\dot{T}_2 - Q_{diff20} \\ + Q_{diff12} + Q_{adv20} = 0 \end{cases} \quad (20)$$

at the top node of the element.

Together with Equations (18)–(20) additional equations are necessary in order to describe the mass flow rates within the ventilation layer. Assume that the full inlet pressure p^+ , the partial pressure, p_{v1}^+ , of water vapor at the inlet, the ventilation volumetric flow rate, v^+ , and gas temperature, T^+ , at the inlet are known. The mass flow rates of the supplied air and water vapor can be obtained as

$$w_{v1}^+ = \frac{v^+ p_{v1}^+ \mu_v}{RT_\infty}; \quad w_{a1}^+ = \frac{v^+ p_{a1}^+ \mu_a}{RT_\infty}. \quad (21)$$

where $p_{a1}^+ = p^+ - p_{v1}^+$ is the partial pressure of the air at the inlet of the ventilation layer.

We consider the freely open ventilation outlet, therefore the average full pressure in the ventilation layer is

$$p^* = \frac{1}{2}(p^+ + p^\infty), \quad (22)$$

where p^∞ is the full pressure in the external environment.

Alternatively the average pressure in the ventilation layer can be expressed as the sum of partial pressures of air and water vapor as

$$p^* = p_{a0} + p_{v0} = \frac{m_{v0} RT_1}{\mu_v h_t A} + \frac{m_{a0} RT_1}{\mu_a h_t A}. \quad (23)$$

Assume that the air and water vapor, which is supplied into the ventilation layer through the inlet is fully mixed with the air and water vapor, which finds the way into the ventilation layer through permeable top and bottom surfaces of the ventilation layer. Therefore we assume that the amounts of the air and water vapor, w_{a0}^- , w_{v0}^- , at the outlet of the ventilation layer are proportional to the amounts of the air and water vapor, m_{a0} , m_{v0} , momentarily contained in the ventilation layer:

$$\frac{w_{v0}^-}{w_{a0}^-} = \frac{m_{v0}}{m_{a0}}. \quad (24)$$

Equations (18)–(20), (23) and (24) comprise the full equation system of the ventilation layer finite element.

After eliminating algebraically the unknown flow rates, w_{a0}^-, w_{v0}^- , the equation system reads as

$$\begin{cases}
 \dot{m}_{v1} = -\tilde{\delta}_p A(p_{v1} - p_{v0}) + w_{v1}; \\
 \dot{m}_{a1} = -\tilde{k}_a A(p_{a1} - p_{a0}) + w_{a1}; \\
 (c_a m_{a1} + c_v m_{v1}) \dot{T}_1 = Q_{adv01} - \tilde{\alpha} A(T_1 - T_0) \\
 \quad - \alpha_{3D} A(T_1 - T_2) + \hat{Q}_1 + c_v \hat{w}_{v1} T_{human}; \\
 \dot{m}_{v2} = -\tilde{\delta}_p A(p_{v2} - p_{v0}) + w_{v2}; \\
 \dot{m}_{a2} = -\tilde{k}_a A(p_{a2} - p_{a0}) + w_{a2}; \\
 (c_a m_{a2} + c_v m_{v2}) \dot{T}_2 = Q_{adv02} - \tilde{\alpha} A(T_2 - T_0) \\
 \quad + \alpha_{3D} A(T_1 - T_2) + Q_2; \\
 m_{a0} \dot{m}_{v0} - m_{v0} \dot{m}_{a0} = m_{a0} w_{v0}^+ - m_{v0} w_{a0}^+ \\
 \quad + m_{a0} \tilde{\delta}_p A(p_{v1} + p_{v2} - 2p_{v0}) - m_{v0} \tilde{k}_a A(p_{a1} + p_{a2} - 2p_{a0}); \\
 \frac{\dot{m}_{v0}}{\mu_v} + \frac{\dot{m}_{a0}}{\mu_a} + \frac{p * h_0 A}{R(T_0)^2} \dot{T}_0 = 0; \\
 -\dot{m}_{v0} c_v T_0 - \dot{m}_{a0} c_a T_0 + (c_a m_{a0} + c_v m_{v0} + c_{3D} A) \dot{T}_0 \\
 = Q_{adv10} + Q_{adv20} + \tilde{\alpha} A(T_1 + T_2 - 2T_0) \\
 + (c_v w_{v0}^+ + c_a w_{a0}^+) T^{+-} - \\
 -c_v w_{v0}^+ T_0 - c_v \tilde{\delta}_p A(p_{v1} - p_{v0}) T_0 \\
 -c_v \tilde{\delta}_p A(p_{v2} - p_{v0}) T_0 - c_a w_{a0}^+ T_0 - c_a \tilde{k}_a A(p_{a1} - p_{a0}) T_0 \\
 -c_a \tilde{k}_a A(p_{a2} - p_{a0}) T_0.
 \end{cases} \tag{25}$$

Equation system (25) in matrix form reads as

$$\begin{bmatrix}
 m_{a0} & -m_{v0} & 0 & 0 & 0 & 0 & 0 \\
 \frac{1}{\mu_v} & \frac{1}{\mu_a} & \frac{p * h_0 A}{R(T_0)^2} & 0 & 0 & 0 & 0 \\
 -c_v T_0 & -c_a T_0 & c_a m_{a0} + c_v m_{v0} + c_{3D} A & 0 & 0 & 0 & 0 \\
 0 & 0 & 0 & 1 & 0 & 0 & 0 \\
 0 & 0 & 0 & 0 & 1 & 0 & 0 \\
 0 & 0 & 0 & 0 & 0 & c_a m_{a1} + c_v m_{v1} & 0 \\
 0 & 0 & 0 & 0 & 0 & 0 & 1 \\
 0 & 0 & 0 & 0 & 0 & 0 & 0 & 1 \\
 0 & 0 & 0 & 0 & 0 & 0 & 0 & 0 & c_a m_{a2} + c_v m_{v2}
 \end{bmatrix}
 \begin{Bmatrix}
 \dot{m}_{v0} \\
 \dot{m}_{a0} \\
 \dot{T}_0 \\
 \dot{m}_{v1} \\
 \dot{m}_{a1} \\
 \dot{T}_1 \\
 \dot{m}_{v2} \\
 \dot{m}_{a2} \\
 \dot{T}_2
 \end{Bmatrix}
 =
 \begin{Bmatrix}
 m_{a0} w_{v0}^+ - m_{v0} w_{a0}^+ + m_{a0} \tilde{\delta}_p A(p_{v1} + p_{v2} - 2p_{v0}) - m_{v0} \tilde{k}_a A(p_{a1} + p_{a2} - 2p_{a0}) \\
 0 \\
 Q_{adv10} + Q_{adv20} + \tilde{\alpha} A(T_1 + T_2 - 2T_0) - (c_v w_{v0}^+ + c_v \tilde{w}_{v1} + c_v \tilde{w}_{v2} + c_a w_{a0}^+ + c_a \tilde{w}_{a1} + c_a \tilde{w}_{a2}) T_0 \\
 -\tilde{w}_{v1} \\
 -\tilde{w}_{a1} \\
 Q_{adv01} - \tilde{\alpha} A(T_1 - T_0) - \alpha_{3D} A(T_1 - T_2) \\
 -\tilde{w}_{v2} \\
 -\tilde{w}_{a2} \\
 Q_{adv02} - \tilde{\alpha} A(T_2 - T_0) + \alpha_{3D} A(T_1 - T_2)
 \end{Bmatrix}
 +
 \begin{Bmatrix}
 0 \\
 0 \\
 (c_v w_{v0}^+ + c_a w_{a0}^+) T_\infty \\
 \hat{w}_{v1} \\
 0 \\
 \hat{Q}_1 + c_v \hat{w}_{v1} T_{human} \\
 w_{v2} \\
 w_{a2} \\
 Q_2
 \end{Bmatrix}; \tag{26}$$

where $\tilde{w}_{v1}, \tilde{w}_{a1}, \tilde{w}_{v2}, \tilde{w}_{a2}, p_{a1}, p_{v1}, p_{a2}, p_{v2}, Q_{adv10}, Q_{adv20}, Q_{adv01}, Q_{adv02}, Q_{adv12}$ are obtained from the relationships (11), (1),(14) and (15). Pressures p_{a0}, p_{v0} are obtained from the equations

$$p_{a0} = \frac{m_{a0} R T_0}{\mu_a h_0 A}, \quad p_{v0} = \frac{m_{v0} R T_0}{\mu_v h_0 A}. \tag{27}$$

The diagonal terms $(c_a m_{a1} + c_v m_{v1}) \dot{T}_1, (c_a m_{a2} + c_v m_{v2}) \dot{T}_2$ of the left-hand side of the matrix in Equation (26) are the capacity terms corresponding to inter-layer gaps, which are common to each pair of elements of the textile package structure. As the equations of individual elements are joined together to the equation system of the structure, the terms should be added directly to the appropriate positions in the diagonal of the assembled structural capacity matrix of the structure rather than being ‘assembled’ from the matrices of individual finite elements.

Solution scheme

Equations (10) and (26) of finite elements of textile and three-dimensional ventilation layers, which form the structure of the multilayer textile package, are assembled from the structural equation

$$[C(\{U\})][\dot{U}] = \{f(\{U\}, t)\} \tag{28}$$

where $[C(\{U\})]$ is the capacity matrix of the structure, $\{U\} = \{m_{v0}, m_{a0}, T_0, m_{v1}, m_{a1}, T_1, m_{v2}, m_{a2}, T_2, \dots, m_{vn}, m_{an}, T_n\}^T$ is the vector of nodal variables.

The values of real material parameters in most cases determine that (28) is a stiff differential equation because of very different rates of change of masses and temperatures. In this work for the solution of Equation (28) the MATLAB function `ode23tb` has been used.

Parameters of the models

The practical need to analyze the packages made of modern textile materials encounters difficulties because of unknown physical parameter values, such as heat transfer, heat capacity, water vapor transmission and air permeability coefficients, water vapor capacity and others used in the developed model. Many parameters can be measured by using the appropriate standard procedures, such as LST EN 31902:2002 for determining water vapor resistance R_{et} (m^2Pa/W), LST EN ISO 9237:1997 for determining the air permeability coefficient ψ_a (mm/s), LST EN 31902:2002 for determining thermal resistance θ (m^2K/W). The standard procedures are based on well-known physical laws and provide physically meaningful coefficients. The problem is that sometimes the obtained values cannot be used in finite element model equations directly. The following recalculations are necessary.

The water vapor mass transmission coefficient, β_v , cannot be obtained directly by the standard measurement procedure, which defines the *water vapor resistance* as $R_{et} = \frac{A\Delta p}{H}$ (m^2PaW^{-1}), where Δp is the pressure difference measured at the surface of the measuring unit and in the test enclosure, A is the area of the measuring unit and H is the heating power supplied to the measuring unit provided that temperatures at the surface of the measuring unit and in the test enclosure are equal to $35^\circ C$ (for the sake of simplicity here we omitted the apparatus correction terms). The measurement conditions require that at $35^\circ C$, the steady-state pressure difference equals $\Delta p = 5620 Pa - 2250 Pa$, where $2250 Pa$ is the water vapor partial pressure at 40% humidity as required by the standard procedure and $5620 Pa$ is the saturated water vapor partial pressure at the surface of the measurement block. The obtained value cannot be used directly in Equation (3), as the water vapor transmission coefficient should express the flow rate through the unit area caused by the unity pressure difference between the two surfaces. Recalculation is necessary, during which we algebraically eliminate the heat power. At isothermal conditions we assume that the heating power is

transformed to the power of water vapor, which penetrates the textile layer and may write $H = \frac{w_v \Delta p}{\rho_v}$, where ρ_v is the water vapor density at, $35^\circ C$ temperature. In accordance with Equation (3) we have $w_v = \delta_p A \Delta p$. By combining together the three last relationships, we obtain the recalculation formula $\delta_p = \frac{\rho_v}{R_{et} \times (5620 - 2250)}$ (sm^{-1}). Note that R_{et} and δ_p have identical dimensions $\left[\frac{m^2 Pa}{W}\right] = \left[\frac{kg/s}{m^2 Pa}\right] = \left[\frac{s}{m}\right]$.

The air mass permeability coefficient, k_a , which is used in Equation (3), cannot be immediately obtained by means of the standard measurement. The standard procedure provides the *air permeability coefficient* as $\psi_a = \frac{q_v}{A} \left(\frac{mm}{s}\right)$, where q_v is the air flow volumetric rate through the textile layer of area, A , which takes place at a pressure difference of $125 Pa$ on both sides of the material as required by the standard. The air mass permeability coefficient compatible with Equation (3) is obtained as $k_a = \psi_a \times 10^{-3} (ms^{-1}) \times \frac{\rho_a (kgm^{-3})}{125 (Pa)} = \psi_a \times 9.328 \times 10^{-6} (sm^{-1})$, where ρ_a is the air mass density and 10^{-3} is the conversion coefficient from mm to m. The heat transfer coefficient is obtained as the reverse of the thermal resistance as $\alpha_t = \frac{1}{\theta} (Wm^2K^{-1})$.

Some experimental measurement results of materials listed in Table 1 are provided in Table 2. The measurement results provide information about numerical values of the physical coefficients of textile materials, which most significantly influence the processes of heat and mass exchange in textile packages. This information should be regarded as examples of physical properties of textile materials used in real protective clothing. Within the scope of this work we did not make a systematic study about the influence of morphologies and the micro-structure of textile materials on the values of the coefficients.

Values of unknown heat and hydraulic capacity parameters are difficult to measure. Approximate values of them have been calculated on the basis of the values presented by Mashinskaya and Petrov¹⁶ and then adjusted more finely by comparing the numerical simulation results against the results of certain physical experiments. We hope that even with rough estimations of the capacity parameter values, the errors in modeling results are not crucial as they may influence only duration of complex interaction processes rather than the obtained state of thermal and water vapor concentration equilibrium. On the other hand, the innovative solutions of smart textiles provide a wide spectrum of materials with different physical properties, therefore theoretical analysis of

Table 1. The assortment and characteristics of the textile materials used for military clothing

Material	Fibre content	Surface density, g/m ²	Thickness, mm	Description of the material	Linear density, tex	Finishing
1a	Cotton – 100%	120	0.8	Knitted material (interlock)	Cotton yarn 11,8 tex	Printing, softening finishing
1b	Cotton – 92%; Polyester – 6.3%; Elastane – 1.7%	215	1.2	Knitted material (rib) (1x1)	Cotton-Polyester yarn 20 tex; Elastane thread 4.9 tex	Washing-partial bleach, softening finishing
2a	Cotton – 32%; Polyester – 68%	187	0.7	Woven material (rip-stop)	Polyester-Cotton yarn 15x2 tex; Polyester-Cotton yarn 20x2 tex	Printing, hydrophilic finishing
2b	Cotton – 62%; Polyester – 38%	251	0.8	Woven material (rip-stop)	Cotton yarn 20x2 tex; Polyester-Cotton yarn 25x2 tex	Printing, hydrophobic-oleophobic finishing
3	Polyester – 100%	287	4.8	Double faced knitted material (pile)	–	Shearing, antipilling finishing
4	Cotton – 34%; Polyester – 66%	173	0.9	Woven material (plain)	Polyester-Cotton yarn 15x2 tex; Polyester-Cotton yarn 25 tex	Dyeing, softening finishing
5a	I l. –polyester 100%; II l. – polyurethane 100%; III l. –polyamide 100%	219	0.8	Three-layer material with micro pore membrane	I layer textured polyester yarn 24 tex	I layer-printing; Three-layer material has hydrophobic-oleophobic finishing
5b	I l. – polyester 100%; II l. – polyurethane 100%; III l. –polyamide 100%	258	0.9	Three-layer material with micro pore membrane	I layer textured polyester yarn 16.7 tex	I layer-printing. Three-layer material has hydrophobic-oleophobic finishing

the influence of the parameters on wearing comfort conditions are of considerable value.

Numerical results

Analysis of temperatures in the three-dimensional ventilation layer covered by a textile package

Pure heating. The calculations demonstrate the process of heat convection from the three-dimensional textile layer by the ventilation air flow, Figure 3. As the side boundaries of the three-dimensional layer can be treated as a free outlet, the model assumes a constant pressure value within the layer, which is equal to the environment pressure. On the contrary, the gaps between each layer of textiles, as well as, between textiles and the heating plate (human skin) are assumed to be isolated from the environment at their side boundaries. Therefore the pressure within the gaps can vary due to the variation of the temperature. The heat and mass exchange can take place only through the top and bottom of each gap because of the permeability of the neighboring textile surfaces to air, water

vapor and heat. The value of the heat transfer coefficient of the three-dimensional textile layer, $\alpha_{3D} = 8.4746 \text{ Wm}^{-2}\text{K}^{-1}$, is based on measurements in accordance with the standard LST EN 31902:2002, Table 2. The experimental values of constants of the three-dimensional textile layer in reality are the values, which correspond to combined conductivity of the three-dimensional structure itself and of the air, which is always present within the three-dimensional layer. As the model described in section 3 requires the heat conductivity of the three-dimensional structure only, we had to subtract the heat conductivity of the air contained in the three-dimensional layer, which at a thickness of 0.0075 m is equal to $0.0264/0.0075 = 3.52 \text{ Wm}^{-2}\text{K}^{-1}$. Therefore the value used in calculations was $\alpha_{3D} = 4.95 \text{ Wm}^{-2}\text{K}^{-1}$. Unfortunately the value of the coefficient $\tilde{\alpha}_{3D}$ used in the model (see Equation (13)) could not be measured directly by the standard measurement procedures. The coefficient describes the convective heat exchange between the three-dimensional textile material, which is the solid structure containing water vapor and air and the neighboring air–water vapor gas mixture in the inter-layer gap.

Table 2. The characteristics of the textile materials indicated in Table 1

Material	Surface density, g/m^2 , (LST EN 12127:1999)	Thickness, mm	Water vapor transmission coefficient $\phi_p = \frac{q_v}{R_{et} \times (56.20 - 22.50)}$, $m^2 Pa/W = s/m$	Water vapor resistance, R_{et} , $m^2 Pa/W$, (LST EN 31902:2002)	Water vapor absorption % at relative humidity		Air permeability, ψ_a , mm/s, (LST EN ISO 9237:1997)	Air mass permeability coefficient $k_a = R \times 9.328 \times 10^{-6}$ s/m	Thermal resistance, $m^2 K/W$, (LST EN 31902:2002)	Heat transfer coefficient $Wm^{-2}K^{-1}$
					100%	40%				
1a	120	0.8	0.5946 e-3	0.37	8.3	5.2	1629	0.0152	0.025	40.
1b	215	1.2	0.0541 e-3	4.07	7.3	5.5	652	0.0061	0.035	28.5714
2a	187	0.7	0.5116 e-3	0.43	3.4	2.4	122	0.0011	0.007	142.8571
2b	251	0.8	0.0701 e-3	3.14	5.3	3.2	60	0.0006	0.008	125.
3	287	4.8	0.0168 e-3	13.11	0.9	0.3	666	0.0062	0.147	6.8027
4	173	0.9	0.1089 e-3	2.02	3.5	2.1	234	0.0022	0.023	43.4783
5a	219	0.8	0.0195 e-3	11.31	1.8	0.4	0	0	0.005	200.
5b	258	0.9	0.0230 e-3	9.57	2.3	1.1	0	0	0.006	166.6667
Twaron LFT GF4	5300	6	0	0	0	0	0	0	0.183	5.46
Twaron CT709	6400	9.6	0	0	0	0	0	0	0.124	8.06
Dyneema	5300	7.3	0	0	0	0	0	0	0.132	7.56
3D textile	520	7.5	3.4589 e-005	6.36	-	-	404	0.00475	0.118	8.4746

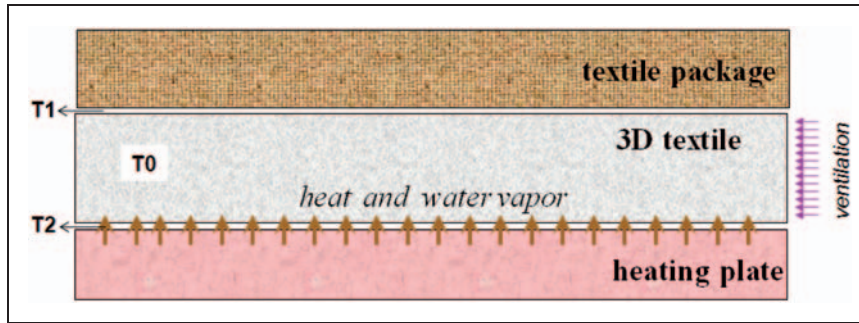


Figure 3. Experimental scheme of measurement of heat convection from the textile multilayer by three-dimensional textile ventilation layer.

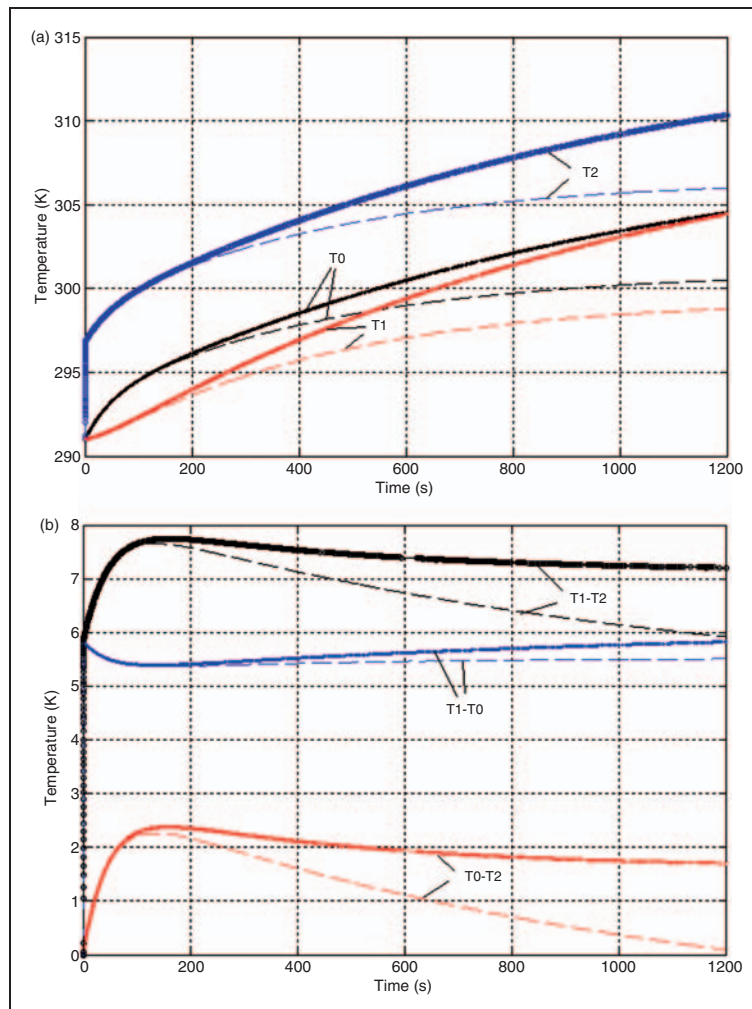


Figure 4. Air temperatures (a) and differences of temperatures (b) at the ventilated three-dimensional textile layer; pure heating power 35 W, outer surface covered by Twaron CT709 textile package, outer temperature 291 K. Material constants $\alpha_{3D} = 4.95 \text{ Wm}^{-2}\text{K}^{-1}$; $\tilde{\alpha}_{3D} = 20 \text{ Wm}^{-2}\text{K}^{-1}$; $c_{3D} = 1800 \text{ Wm}^{-2}\text{K}^{-1}$; $\alpha_{package} = 8.06 \text{ Wm}^{-2}\text{K}^{-1}$; area 0.24 m^2 ; ———, no ventilation; - - - -, ventilation $92 \text{ dm}^3 \text{ min}^{-1}$.

Moreover, its surfaces do not fully isolate the inside gas from the gas in the inter-layer gap. In this model, we treated the ventilation layer as 'like a solid body' and chose the convection heat transfer coefficient less than usually used for similar solid materials. We believed

$\tilde{\alpha}_{3D} = 20 \text{ Wm}^{-2}\text{K}^{-1}$ was a close-to-reality value, moreover, it produced reasonable results as experimentally measured temperatures inside and outside of the ventilation layer were compared with each other.

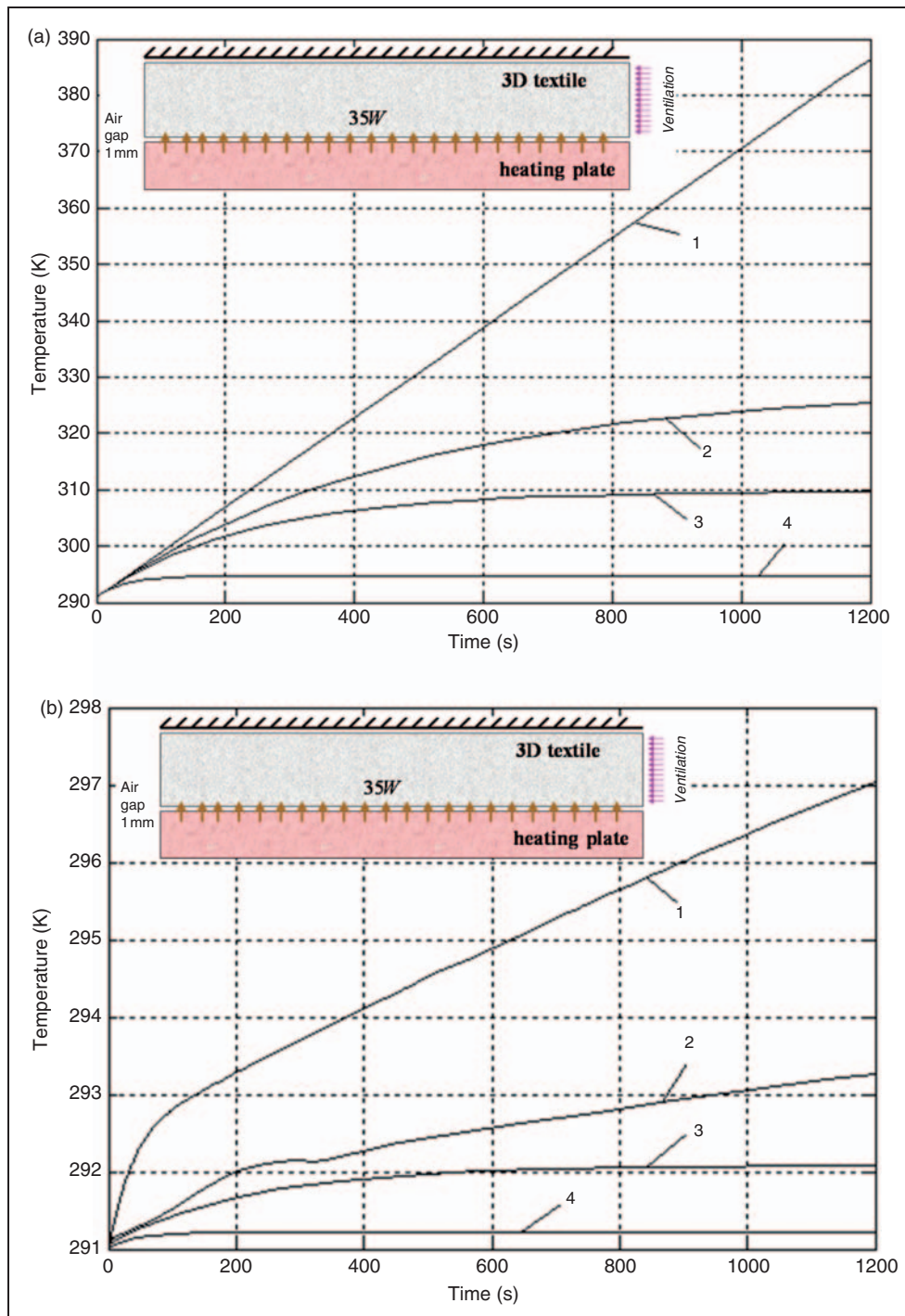


Figure 5. Air temperature time laws in ventilated three-dimensional textile layer with thermally isolated outer side. Pure heating 35 W in absolutely dry air (a) and heating by water vapor equivalent to 35 W at partial pressure of water vapor in environment air 1000 Pa (b): 1, no ventilation; 2, 46 Lmin⁻¹; 3, 92 Lmin⁻¹; 4, 460 Lmin⁻¹; area 0.24 m².

The heat capacity value $c_{3D} = 1800 \text{ Jm}^{-3}\text{K}^{-1}$ is also selected in order to obtain the time law of temperature increase close to experimental. On the other hand, the heat capacity value does not influence the final temperature value when the state of thermal equilibrium is reached. Permeability coefficients of the top and bottom surface of the three-dimensional textile layer to water vapor and air are $\delta_p = 3.4589 \times 10^{-3} \text{ m}^2 \text{ PaW}^{-1}$; $k_a = 0.0475 \text{ m}^2 \text{ PaW}^{-1}$.

The time laws of the air temperature in the ventilation layer (T0), in the gap at the textile package Twaron CT709 (T1) and at the heating plate (T2) have been calculated at given ventilation rates $v^+ = 0$ and $v^+ = 92 \text{ dm}^3 \text{ min}^{-1}$, Figure 4. Notice that even in the absence of the ventilation air flow, the temperature differences T1–T0 and T2–T0 do not converge to zero because of different pressures in the three-dimensional textile layer and in the neighboring inter-layer gaps.

Analysis of temperatures in the three-dimensional textile ventilation layer and in the microclimate gap at isolated outer surface

Figure 5 demonstrates the time laws of temperature increase in the three-dimensional textile layer, when no heat and mass exchange through the top surface is possible and heat (no water vapor) of 35 W is applied to the bottom surface. If we assume that the three-dimensional textile layer is not permeable to water vapor and air ($\delta_p = k_a = 0$), the thermal equilibrium situation, which is reached after a sufficiently long time period can be obtained from Equation (26) as $T_0 = T_\infty \left(1 + \frac{\dot{Q}_1 R}{v^+(c_v p_{v1}^+ \mu_v + c_a p_{a1}^+ \mu_a)} \right)$, which is independent of the physical constants of the three-dimensional textile layer. However, the physical constants of the three dimensional textile layer determine the properties of the

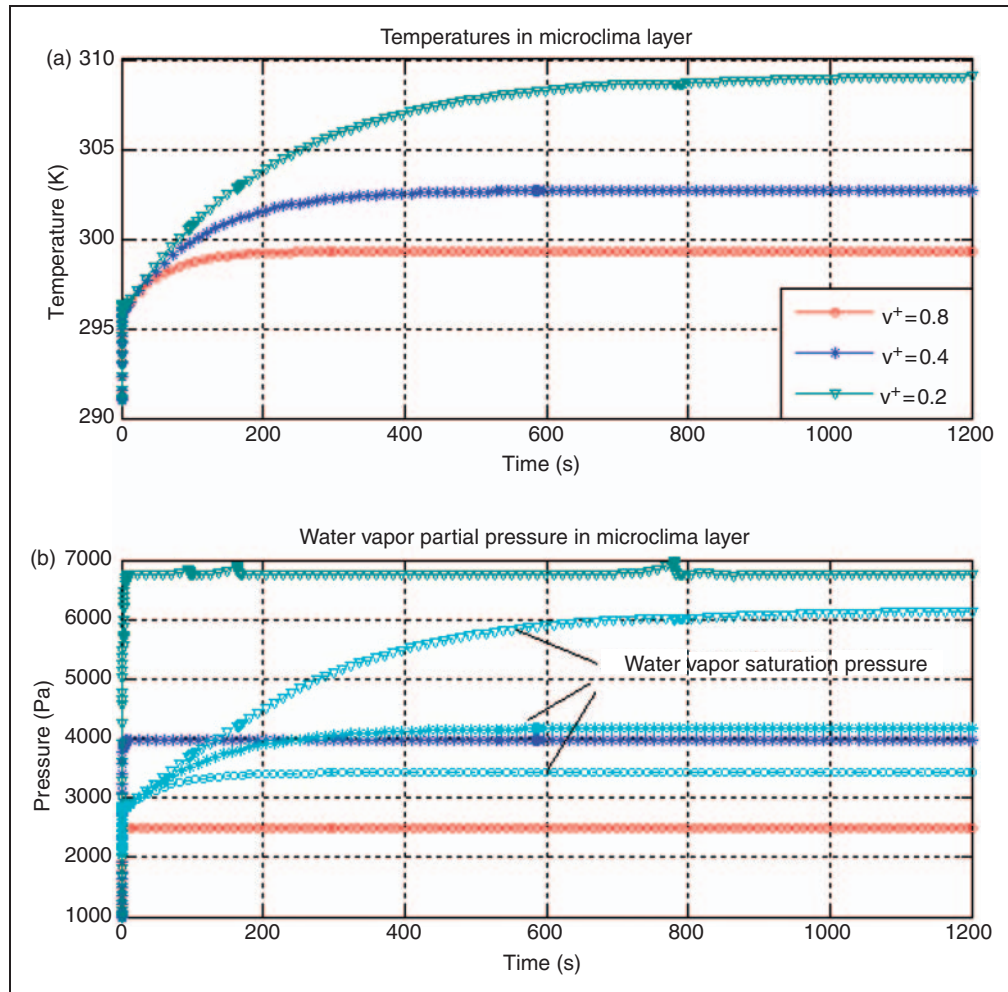


Figure 6. Time relationships of temperatures (a) and partial water vapor pressures (b) in the microclimate gap at three different values of the ventilation rate 0.2, 0.4 and 0.8 dm³ min⁻¹ if the surface of the ventilation layer is fully isolated from outside. Heating by vapor of temperature 310 K, and equivalent power 35 W, and simultaneous additional heating of 25 W.

temperature time law. The steady temperatures in the bottom and top gaps near the three-dimensional textile layer are obtained as $T_1 = T_0 + \frac{\dot{Q}_1}{A} \frac{\alpha + \alpha_{3D}}{\alpha(\tilde{\alpha} + 2\alpha_{3D})}$; $T_2 = T_0 + \frac{\dot{Q}_1}{A} \frac{\alpha_{3D}}{\alpha(\tilde{\alpha} + 2\alpha_{3D})}$. At a heating power value of 10 W, a volumetric rate of 92 Lmin⁻¹ and the temperature of the air supply to the three-dimensional textile layer at 291K, we obtain $T_0 = 296.344$ K, $T_1 = 298.08$ K, $T_2 = 296.69$ K.

Assume that a water vapor temperature of 310K is generated at the human skin and three-dimensional textile interface (microclimate gap). The analysis is reasonable if top and bottom surfaces of the

three-dimensional textile layer are permeable to the water vapor by considering the permeability coefficient $\delta_p = 3.4589 \times 10^{-3} \text{ m}^2\text{PaW}^{-1}$. In the three-dimensional textile layer water vapor is mixed with the ventilation air and driven out of the layer. The water vapor generated by human skin surface increases partial water vapor pressure in the microclimate gap, as well as, supplies heat power, $c_v \hat{w}_{v1} T_{human}$, where \hat{w}_{v1} is the mass rate of the generated vapor, T_{human} is the temperature of the vapor, which we assume to be 310 K. Figure 5b demonstrates the temperature time laws of the outgoing ventilation air under similar equivalent heating power conditions as in Figure 5a. Lower temperatures

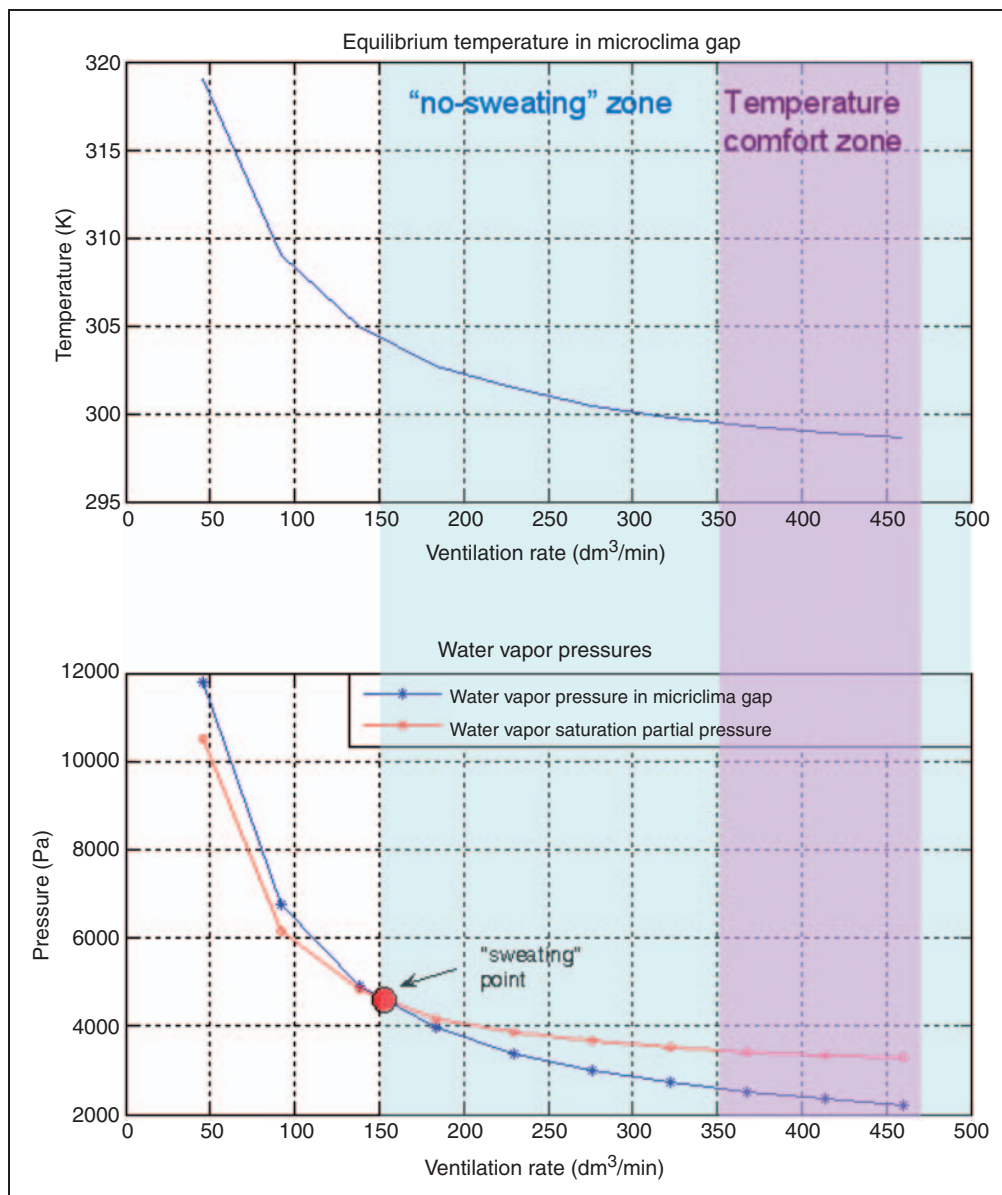


Figure 7. Equilibrium temperature (a) and water vapor partial pressure (b) in the microclima gap against the ventilation rate.

observed in the relationships in Figure 6 are caused mainly by the transport of heat power by means of the water vapor penetration into the three-dimensional textile layer through its bottom boundary.

Calculating ventilation rates and predicting sweating situations

As the model can be used to obtain the water vapor partial pressures and temperatures in inter-layer gaps, the sweating situations can be predicted if the saturated water vapor is obtained. Figure 6 presents examples of time relationships of temperatures and partial water vapor pressures in the microclimate gap and at the isolated outer surface of the three-dimensional textile ventilation layer. Three pairs of lines are observed in Figure 6b, which present the water vapor partial pressures and the water vapor saturation pressures at temperature values taken from the temperature

relationships of Figure 6a. We assumed that the human skin (heating plate) generates the water vapor of temperature 310 K and equivalent power 35 W and simultaneously additional heating of 25 W. The outside air temperature is 291 K. Sweating takes place if the pressure curve is above the saturation pressure curve. As in Figure 6, the curves marked by circles correspond to no-sweating situations and are close to optimum with the equilibrium temperature of 299 K. Curves marked by asterisks correspond to the sweating limit, with an equilibrium temperature of 303 K and sweating during the first 300 s. Curves marked by v-markers indicate an unacceptable situation of strong overheating of 309 K and sweating.

Figure 7 presents the dependencies of equilibrium temperature and water vapor partial pressure in the microclimate gap against the ventilation rate. The intersection of the water vapor partial pressure and the saturated vapor pressure curves in Figure 7b provides the

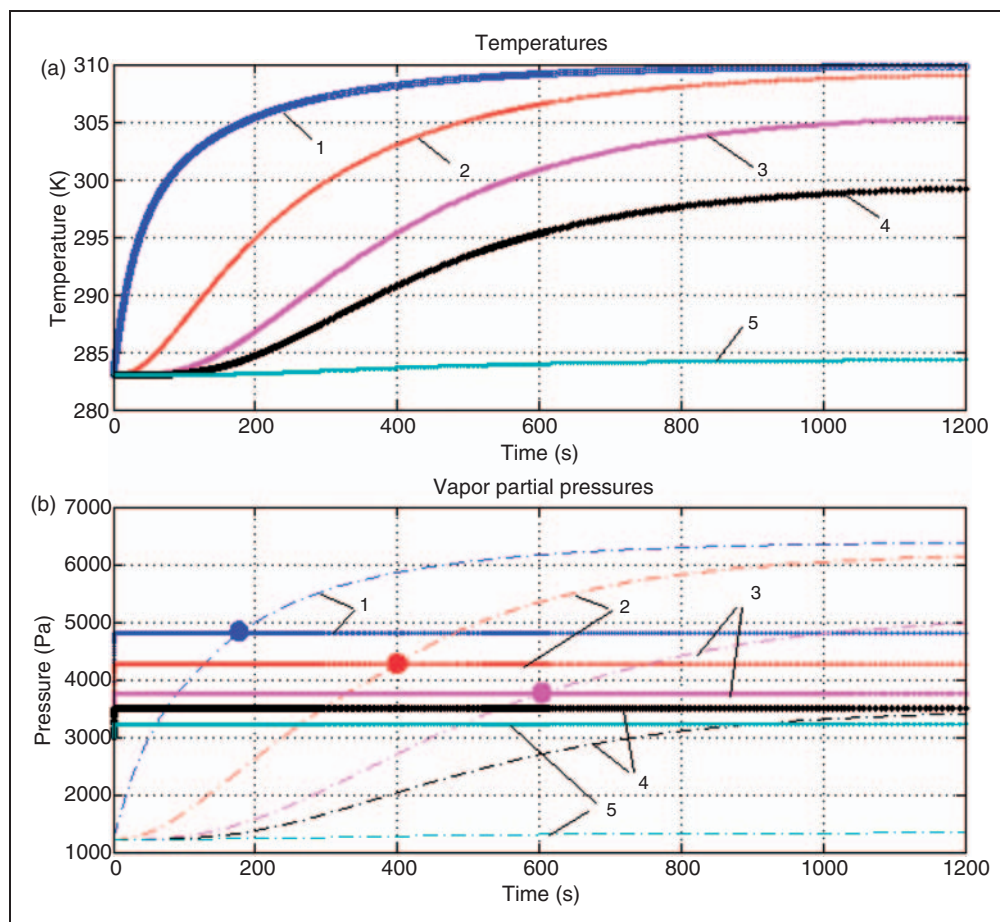


Figure 8. Temperatures (a) and water vapor partial pressures (b) between layers of the permeable textile package (materials 3 + 3 + 3 + 3 + 3 + 3 + 5a. Table 2). Dots indicate water vapor saturation points in gaps between two layers. Heating by vapor of temperature, 310 K; power, 750 W; environment temperature, 290 K; partial water vapor pressure in the environment air, 3000 Pa. 1, 1st gap (microclimate); 2, 3rd gap; 3, 5th gap; 4, 6th gap; 5, 7th gap.

minimum value of the ventilation rate, below which steady sweating takes place. The range of acceptable ventilation rates is determined, which covers the intersection of no-sweating and temperature comfort zones.

Analysis of temperatures and mass exchange in permeable multi-layers

Figure 8 presents the main quantities, which characterize the heat and mass exchange in 7-layered textile multilayers that are non-ventilated and permeable to water vapor and heat. The structure of the multilayer is made of the materials 3+3+3+3+3+3+5a presented in Table 2. Figure 8a presents time laws of temperature in inter-layer gaps. Solid lines in Figure 8b present water vapor partial pressures in the microclimate gap and in the subsequent gaps. Dashed lines in Figure 8b present the saturated water vapor partial pressures at temperatures, which correspond to the time laws in Figure 8a. Intersections of curves in Figure 8b (big dots) indicate the sweating limit points. It may be noticed that in the 6th and 7th gaps, the water vapor partial pressure exceeds the saturation pressure all the time, while in gaps closer to the heating and evaporation plate a steady no-sweating situation is obtained after certain periods of time.

Conclusion

A new structural model has been developed, which enables the analysis of air and water vapor mass and heat exchange in multilayer textile packages widely used in military and protective clothing. The model is uni-dimensional, each element of which describes a single layer of the package. Most parameters of the model can be obtained by performing standard measurements. Values of some parameters were adjusted by comparing experimental data with numerical calculations. The model enabled the temperatures between each pair of textile layers to be obtained, as well as, in the three-dimensional textile forced ventilation layer. The time point of sweating could be calculated for any combination of textile materials in the package.

Though the model is able to take into account the principal air and water vapor flow rates and heat fluxes through all layers of the multilayer textile package, some points still remain hypothetical and provide space for future research. The finite element of the three-dimensional textile ventilation layer is highly simplified in comparison with the geometrically complex internal structure and tends to display only the main processes, which could influence the wearing comfort conditions. At the moment we could not measure the exact convective heat transfer coefficient at the surfaces of the layer and relied on indirect comparisons of certain computed

results against the experimental ones. Future studies and corresponding finite element models could be useful in order to analyze the mass and heat transfer processes at the micro-scale, which could provide more reliable information about the equivalent coefficients necessary for the macro-scale finite element model described in this paper. The ventilation gas flux and pressure distribution in real geometries of the clothes are also important issues, as well as, water vapor condensation effects. The innovative solutions of smart textiles provide a wide spectra of materials with different physical properties, therefore the theoretical analysis of influence of the parameters on wearing comfort conditions are of considerable value. Another important study could be a systematic research on the influence of morphologies and micro-structure of textile materials on the values of the physical coefficients, which have most significant influence on the heat and mass exchange processes in textile materials.

Funding

This work was partly supported by the Lithuanian State Science and Studies Foundation (grant number B-18/2007).

List of symbols

Geometrical

h_t (m)	thickness of the textile layer;
h_{g1}, h_{g2} (m)	sizes of the gaps at both sides of the textile layer;
h_0 (m)	thickness of the three-dimensional spacer fabric ventilation layer;
A (m ²)	area of the textile layer;

Physical constants and coefficients

$R = 8.314472$ Jmol ⁻¹ K ⁻¹	the universal gas constant;
$\mu_v = 0.018$ kg	molar mass of water vapor;
$\mu_a = 0.029$ kg	molar mass of air;
c_{ht} (s ² m ⁻¹)	hydraulic capacity of the textile layer, which describes the ability of the unity area of the textile layer to accumulate the water vapor;
δ_p (sm ⁻¹)	coefficient of water vapor transmission, which is defined as the ratio between the density of vapor flow through the textile layer and the magnitude of difference of pressures at both sides of the layer;

$k_a(\text{sm}^{-1})$	coefficient of air permeability, which is defined as the ratio between the density of air flow through the textile layer and the magnitude of difference of pressures at both sides of the layer;		the gaps at both sides of the textile layer;
$c_v(\text{Jkg}^{-1}\text{K}^{-1})$	specific (mass) heat capacity coefficient of water vapor;	$T_0(\text{K})$	temperature of gas in the ventilation layer;
$c_a(\text{Jkg}^{-1}\text{K}^{-1})$	specific heat capacity coefficient of air;	$T_{human}(\text{K})$	temperature of the water vapor produced by the human skin;
$c_t(\text{Jm}^{-2}\text{K}^{-1})$	heat capacity coefficients of the unity area of the textile layer;	$T^+(\text{K})$	temperature of the air and water vapor mixture at the inlet of the ventilation layer;
$\alpha_t(\text{Wm}^{-2}\text{K}^{-1})$	the heat transfer coefficient of the unity area of the textile layer;	$p_{v1}, p_{v2}(\text{Pa})$	partial pressures of the water vapor in the gaps at both sides of the textile layer;
$\alpha_{3D}(\text{Wm}^{-2}\text{K}^{-1})$	heat transfer coefficient used in order to quantify the basically diffusive heat flux Q_{diff12} between the nodes 1 and 2 at both sides of the ventilation layer through the solid structure of the three-dimensional textile material (ventilation layer);	$p_{v0}(\text{Pa})$	partial pressure of the water vapor in the ventilation layer;
$\tilde{\alpha}_{3D}(\text{Wm}^{-2}\text{K}^{-1})$	heat transfer coefficient used in order to quantify the convective heat exchange between the gas in three-dimensional textile material, which is the solid structure containing water vapor and air, and the neighboring air-water vapor gas mixture in the inter-layer gap.	$p_{a1}, p_{a2}(\text{Pa})$	partial pressures of the air in the gaps at both sides of the textile layer;
		$p_{a0}(\text{Pa})$	partial pressure of the air in the ventilation layer;
		$p^+(\text{Pa})$	full pressure at the inlet created by the ventilator;
		$p_{v1}^+(\text{Pa})$	partial pressure of water vapor at the inlet;
		$p_{a1}^+(\text{Pa})$	partial pressure of the air at the inlet of the ventilation layer;
		$p^\infty(\text{Pa})$	full pressure in the external environment;
		$p^*(\text{Pa})$	full pressure in the ventilation layer;
		$\hat{w}_{v1}, \hat{w}_{v2}(\text{kgs}^{-1})$	the nodal flow rates of water vapor, which is accumulated in the yarns of the textile layer;
		$\tilde{w}_v, \tilde{w}_a(\text{kgs}^{-1})$	the flow rates of water vapor and air, which penetrate through the textile layer;

Nodal and element variables of finite elements

$m_{v1}, m_{v2}(\text{kg})$	masses of water vapor contained in the gaps at both sides of the textile layer;	$\tilde{w}_{v1}, \tilde{w}_{a1}, \tilde{w}_{v2}, \tilde{w}_{a2}(\text{kgs}^{-1})$	the flow rates of water vapor and air through the bottom and top surfaces of the three dimensional ventilation layer to the gaps at both sides of the layer;
$m_{v0}(\text{kg})$	mass of water vapor contained in the ventilation layer;		
$m_{a1}, m_{a2}(\text{kg})$	masses of air contained in the gaps at both sides of the textile layer;	$w_{a1}, w_{v1}, w_{a2}, w_{v2}(\text{kgs}^{-1})$	the flow rates of water vapor and air transferred to the gaps from adjacent textile layers or from the human skin;
$m_{a0}(\text{kg})$	mass of air contained in the ventilation layer;		
$T_1, T_2(\text{K})$	temperatures of gas (water vapor and air mixture) in	$w_{a0}^+, w_{v0}^+(\text{kgs}^{-1})$	the flow rates of water vapor and air supplied to

	the inlet of the three-dimensional ventilation layer by the ventilator;	
w_{a0}^-, w_{v0}^- (kgs ⁻¹)	the flow rates of water vapor and air leaving the three-dimensional ventilation layer through the outlet;	\hat{Q}_1 (W)
\hat{w}_{v1} (kgs ⁻¹)	mass flow rate of the water vapor generated by the human skin;	Q_{in}, Q_{out} (W)
v^+ (m ³ s ⁻¹)	the ventilation volumetric flow rate;	
w_{v1}^+, w_{a1}^+ (kgs ⁻¹)	mass flow rates of water vapor and air supplied to the inlet of the ventilation layer;	
Q_{diff} (W)	the heat flux through the textile layer determined by the combined conduction-convection heat transfer mechanism;	
Q_{cap1}, Q_{cap2} (W)	the heat fluxes at both sides of the textile layer created by the flow rate of water vapor, which is accumulated in the yarns of the textile layer and by the thermal capacity of the textile layer;	
Q_{adv1}, Q_{adv2} (W)	the convection heat fluxes at both sides of the textile layer created by the water vapor and air flow rates from the textile to layer to the inter-layer gaps;	
Q_1, Q_2 (W)	the heat fluxes from the adjacent textile layers;	
Q_{diff12} (W)	the diffusive heat flux determined by thermal conductivity of the solid structure of the ventilation layer;	
Q_{conv10}, Q_{conv20} (W)	the convective heat fluxes through the bottom and top surfaces of the ventilation layer;	
Q_{adv01}, Q_{adv10} (W)	the convective heat fluxes at both sides of the textile layer created by the water vapor and air flow rates through the bottom surface of the three-dimensional layer;	
Q_{adv02}, Q_{adv20} (W)	the convective heat fluxes at both sides of the textile layer created by the water vapor and air flow rates through the top surface of the three-dimensional layer;	
	heat power produced by the human skin;	
	heat power contained in the mass flow rates $w_{v0}^+, w_{a0}^+, w_{v0}^-, w_{a0}^-$ through the inlet and outlet of the ventilation layer.	

References

1. Barauskas R and Abraitienė A. Computational analysis of impact of a bullet against the multilayer fabrics in LSDYNA. *Int J Impact Eng* 2007; 34(7): 1286–1305.
2. Li Y and Zhu O. A model of heat and moisture transfer in porous textiles with phase change materials. *Textile Res J* 2004; 75(5): 447–457.
3. Fengzhi L and Yi L. A computational analysis for effects of fibre hygroscopicity on heat and moisture transfer in textiles with PCM microcapsules. *Model Simulat Mater Sci Eng* 2007; 15: 223–235.
4. Ren YJ and Ruckman JE. Condensation in three-layer waterproof breathable fabrics for clothing. *Int J Cloth Sci Technol* 2004; 16(3): 335–347.
5. Ghaddar N, Ghali K and Jones B. Convection and ventilation in fabric layers. In: Pan N and Gibson B (eds) *Thermal and moisture transport in fibrous materials*. CRC Press, 2006, pp.271–307.
6. Ghaddar N, Ghali K and Jones B. Modeling of heat and moisture transport by periodic ventilation of thin cotton fibrous media. *Int J Heat Mass Transfer* 2002; 45: 3703–3714.
7. Ghaddar N, Ghali K, Harathani J and Jaroudi E. Ventilation rates of micro-climate air annulus of the clothing-skin system under periodic motion. *Int J Heat Mass Transfer* 2005; 48: 3151–3166.
8. Oh A. The measurement of water vapour transfer rate through clothing system with air gap between layers. *Int J Heat Mass Transfer* 2008; 44: 375–379.
9. Rossi RM, Gross R and May H. Water vapor transfer and condensation effects in multilayer textile combinations. *Textile Res J* 2004; 74(1): 1–6.
10. Sun Z and Pan Z. Thermal conduction and moisture diffusion in fibrous materials. In: Pan N and Gibson B (eds) *Thermal and moisture transport in fibrous materials*. CRC Press, 2006, pp.225–270.
11. Bhattacharjee D and Kothari VK. Heat transfer through woven textiles. *Int J Heat Mass Transfer* 2008; 44: 375–379.
12. Fukazawa T, Kawamura H, Tochiyama Y and Tamur T. Water vapor transport through textiles and condensation in clothes at high altitudes—Combined influence of temperature and pressure simulating altitude. *Textile Res J* 2003; 73: 657–663.
13. Knitting International. ‘Breathing Room’. *Knit Americas*. 2002, <http://www.inteletex.com/Featuredetail.asp?PubID=27&NewsId=191>.

14. Barauskas R, Abraitienė A, and Vilkauskas A. Structural model of heat and water vapour exchange in multilayer textile packages, *Vibroengineering 2008, Proceedings of 7th International Conference*, ISSN 1822-1262, *Technologija*, Kaunas University of Technology, 2008, pp.1–5.
15. Zienkiewicz OC and Taylor RL. *The finite element method*. 5th ed. Volume 1, The basis. Oxford: Butterworth-Heinemann, 2000, p.698.
16. Mashinskaya GP and Petrov BV. Principles of developing organic-fibre-reinforced plastics for aircraft engineering. In: Shalin RE (ed.) *Polymer matrix composites*. London: Chapman and Hall, 1995, pp.305–422.